High Coulombic efficiency aluminum-ion battery using an $AlCl_3$-urea ionic liquid analog electrolyte

Michael Angell[a], Chun-Jern Pan[a,b], Youmin Rong[a], Chunze Yuan[a], Meng-Chang Lin[c], Bing-Joe Hwang[b,d], and Hongjie Dai[a,1]

[a]Department of Chemistry, Stanford University, Stanford, CA 94305; [b]Department of Chemical Engineering, National Taiwan University of Science and Technology, Taipei 10607, Taiwan; [c]College of Electrical Engineering and Automation, Shandong University of Science and Technology, Qingdao 266590, People's Republic of China; and [d]National Synchrotron Radiation Research Center, Hsinchu 300, Taiwan

Contributed by Hongjie Dai, December 15, 2016 (sent for review December 1, 2016; reviewed by George Zheng Chen and Xiaolin Li)

In recent years, impressive advances in harvesting renewable energy have led to a pressing demand for the complimentary energy storage technology. Here, a high Coulombic efficiency (∼99.7%) Al battery is developed using earth-abundant aluminum as the anode, graphite as the cathode, and a cheap ionic liquid analog electrolyte made from a mixture of $AlCl_3$ and urea in a 1.3:1 molar ratio. The battery displays discharge voltage plateaus around 1.9 and 1.5 V (average discharge = 1.73 V) and yielded a specific cathode capacity of ∼73 mAh g^{-1} at a current density of 100 mA g^{-1} (∼1.4 C). High Coulombic efficiency over a range of charge–discharge rates and stability over ∼150–200 cycles was easily demonstrated. In situ Raman spectroscopy clearly showed chloroaluminate anion intercalation/deintercalation of graphite (positive electrode) during charge–discharge and suggested the formation of a stage 2 graphite intercalation compound when fully charged. Raman spectroscopy and NMR suggested the existence of $AlCl_4^-$, $Al_2Cl_7^-$ anions and $[AlCl_2{\cdot}(urea)_n]^+$ cations in the $AlCl_3$/urea electrolyte when an excess of $AlCl_3$ was present. Aluminum deposition therefore proceeded through two pathways, one involving $Al_2Cl_7^-$ anions and the other involving $[AlCl_2{\cdot}(urea)_n]^+$ cations. This battery is a promising prospect for a future high-performance, low-cost energy storage device.

aluminum-ion battery | urea electrolyte | ionicity | ionic liquid | energy storage

Cheap, high-rate (fast charge/discharge) rechargeable batteries with long cycle lives are urgently needed for grid-scale storage of renewable energy, as it is becoming increasingly important to replace fossil fuels (1). Lithium-ion batteries (LIBs) are expensive and have limited cycle life, which makes them nonideal for grid-scale energy storage. Furthermore, high-rate capability is necessary for use in the grid, under which conditions LIBs become increasingly unsafe due to the flammability of the electrolytes used. Batteries based on aluminum offer a viable alternative due to aluminum's three-electron redox properties (offers potential for high-capacity batteries), stability in the metallic state, and very high natural abundance. Furthermore, the development of these batteries based on nonflammable electrolytes of low toxicity is critical for minimizing safety hazard and environmental impact. For this reason, ionic liquids (ILs) have been investigated for energy storage due to their low vapor pressure and wide electrochemical windows, unfortunately with the caveat of high cost in most cases. A new class of ionic liquids, referred to as ionic liquid analogs (ILAs) or so-called deep eutectic solvents, generally formed through a mixture of a strongly Lewis acidic metal halide and Lewis basic ligand, have gained significant attention due to their comparable electrochemical and physical properties with reduced cost and minimal environmental footprint (2). Abood et al. first disclosed an ILA derived from the mixture of $AlCl_3$ and an oxygen donor amide ligand (urea or acetamide), in which ions were formed through the heterolytic cleavage of $AlCl_3$ (the Al_2Cl_6 unit) giving $AlCl_4^-$ anions and $[AlCl_2{\cdot}(ligand)_n]^+$ cations, with the latter shown to be responsible for reductive aluminum deposition (3). Since then, numerous different Lewis basic ligands have been shown to form ILAs when mixed with $AlCl_3$, which are capable of effective aluminum deposition (4–6).

Recently, our group developed a secondary Al battery system based on the reversible deposition/stripping of aluminum at the Al negative electrode and reversible intercalation/deintercalation of chloroaluminate anions at the graphite positive electrode in a nonflammable 1-ethyl-3-methylimidazolium chloroaluminate (EMIC-$AlCl_3$) IL electrolyte (7, 8). A ratio of $AlCl_3$/EMIC = 1.3 by mole was used such that $Al_2Cl_7^-$ was present in the (acidic) electrolyte to facilitate aluminum deposition (9). During charging, $Al_2Cl_7^-$ is reduced to deposit aluminum metal, and $AlCl_4^-$ ions intercalate (to maintain neutrality) in graphite as carbon is oxidized. During discharge, this battery exhibited a cathode specific capacity of ∼70 mAh g^{-1} with a Coulombic efficiency (CE) of 97–98%, and ultrahigh charge/discharge rate (up to 5,000 mA g^{-1}) for over 7,000 cycles. However, room for improvement exists as the parameter space for the Al battery remains largely unexplored. The three-electron redox properties of aluminum allow a theoretical specific anode capacity of 2,980 mAh/g, so there is potential for much higher overall capacity (and specific energy) of the battery through the investigation of new cathode and electrolyte materials (10–13). Furthermore, whereas the 97–98% CE of this battery is higher than those of most aqueous battery systems, there is still significant room for improvement. State-of-the-art LIBs are capable of 99.98% CE (14, 15), a benchmark that should be met by alternative battery systems. Another consideration is our existing Al battery electrolyte uses 1-ethyl-3-methylimidazolium chloride (EMIC), which is relatively expensive. Immediately plausible new electrolytes for this system could include any which are capable of reversible aluminum deposition/dissolution. In this work, we investigate the performance of a rechargeable Al battery

Significance

To relieve humanity's dependence on fossil fuels, grid-scale storage of renewable energy must be implemented. This requires cheap, high-rate, and long cycle life energy storage mechanisms. This work presents the development of an Al-ion battery using earth-abundant aluminum and graphite as anode and cathode, respectively, and an ionic liquid analog electrolyte composed of $AlCl_3$ and urea that is very low-cost and eco-friendly. The battery exhibits ∼99.7% Coulombic efficiency and a substantial rate capability, with a cathode capacity of 73 mA g^{-1} at 100 mA g^{-1} (1.4 C).

Author contributions: M.A. and H.D. designed research; M.A., C.-J.P., Y.R., C.Y., and M.-C.L. performed research; M.A. contributed new reagents/analytic tools; M.A., B.-J.H., and H.D. analyzed data; and M.A. and H.D. wrote the paper.

Reviewers: G.Z.C., University of Nottingham; and X.L., Pacific Northwest National Laboratory.

The authors declare no conflict of interest.

[1]To whom correspondence should be addressed. Email: hdai1@stanford.edu.

This article contains supporting information online at www.pnas.org/lookup/suppl/doi:10.1073/pnas.1619795114/-/DCSupplemental.

Downloaded by guest on February 24, 2022

using an ILA electrolyte based on urea, a superior compound in terms of cost (~50× cheaper than EMIC) and eco-friendliness.

Results and Discussion

Cyclic Voltammetry and Galvanostatic Charge/Discharge of Al Battery. The battery cathode was constructed using a graphite powder/polymer binder pasted onto a carbon fiber paper substrate, and the anode was free-standing, high-purity Al foil. $AlCl_3$/urea electrolyte was kept below 40 °C during mixing to avoid electrolyte decomposition. Residual HCl impurities were removed by adding Al foil under heat and vacuum, followed by the addition of ethylaluminum dichloride (*SI Materials and Methods*). Fig. 1 shows the cyclic voltammogram (CV) of the Al and graphite electrodes in the $AlCl_3$/urea (by mole) = 1.3 electrolyte; the ratio we found yielded the battery with the highest capacity with good cycling stability. We observed several graphite oxidation peaks in the 1.6–2.0-V (vs. Al) range, while another well-defined peak appeared at ~2.05 V (Fig. 1*A*). These processes, as well as the corresponding reduction events on the negative sweep, were easily correlated with the galvanostatic charge–discharge curve (Fig. 1*C*) for a battery with ~5-mg cm^{-2} loading of active graphitic material. The redox processes are largely reversible but somewhat kinetically hindered, showing relatively wide peaks (Fig. 1*A*), most likely as a result of the high viscosity of the electrolyte (3). The deposition/dissolution of aluminum (Fig. 1*B*) was also quite reversible, but required some cycling to stabilize (Fig. S1). Based on the aluminum stripping/dissolution reaction and chloroaluminate anion intercalation in graphite, battery mechanisms are suggested and illustrated schematically in Fig. 1*D*.

Fig. 2 shows galvanostatic charge–discharge data for the Al-graphite cell using the $AlCl_3$/urea ILA electrolyte. Initial cycling at 100 mA g^{-1} required ~5–10 cycles for stabilization of the capacity and CE, suggesting side reactions during this time. The CE during first cycle was consistently around 90%, and then (during the first 5–10 cycles) increased above 100% until a stable capacity was reached (at which point CE was stabilized at ~99.7%) (Fig. 2*A*). The phenomenon of CE >100% is unknown to the EMIC-$AlCl_3$ electrolyte system (7) and therefore might involve side reactions with the cationic aluminum species or unbound urea, a topic requiring further investigation. The boxed region of Fig. 2*A* (enlarged in Fig. 2*B*) demonstrates the capacity at varied charge–discharge rate using two different cutoff voltages (2.2 and 2.15 V—chosen based on Fig. 1*A* CV results), after which cycling at 100 mA g^{-1} was resumed until

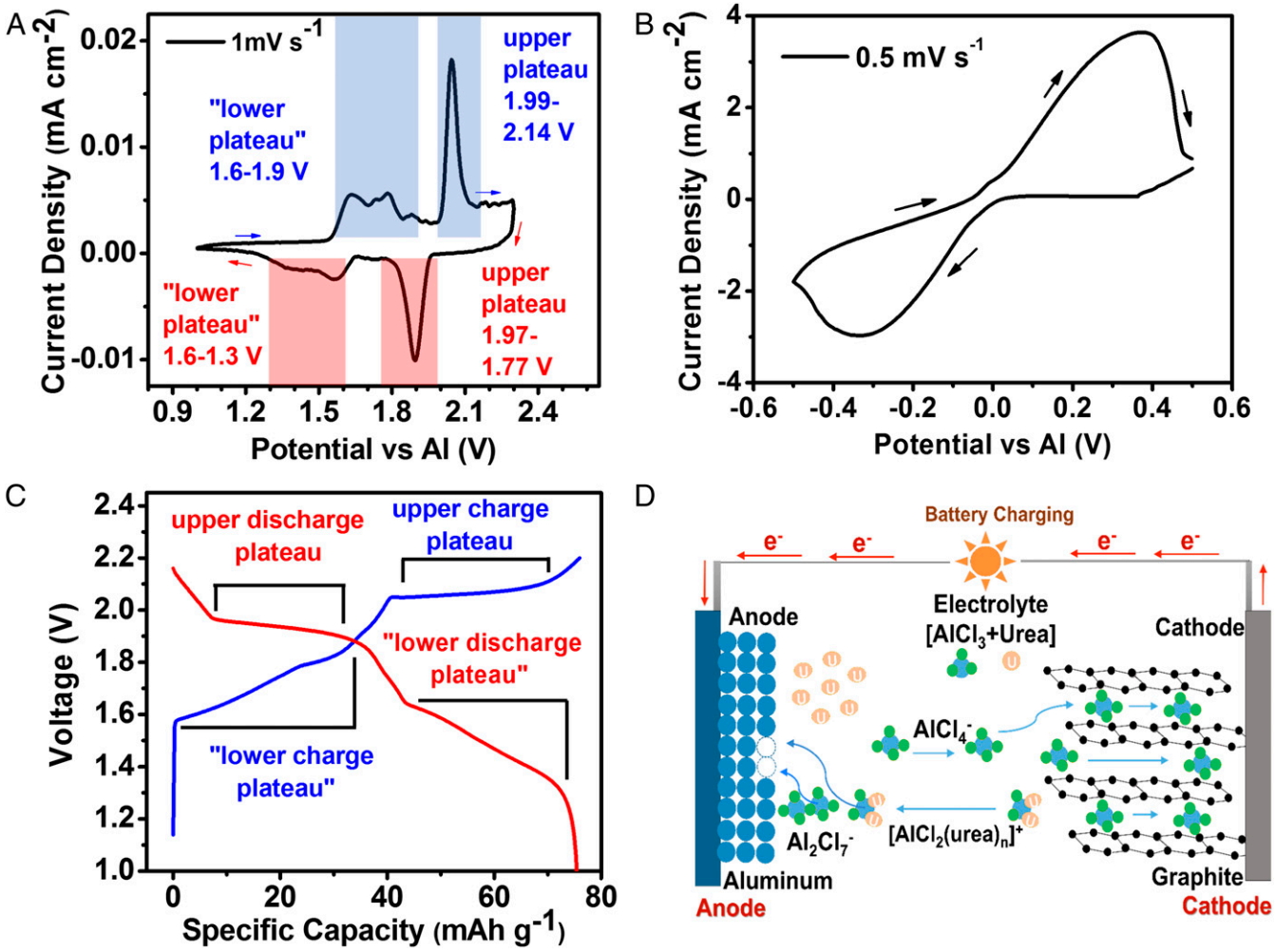

Fig. 1. CV of graphite and aluminum electrodes in $AlCl_3$/urea = 1.3 electrolyte (by mole). (*A*) Graphite intercalation/deintercalation (1 mV s^{-1}), with corresponding major battery charge/discharge curve features indicated. (*B*) Aluminum deposition and stripping (0.5 mV s^{-1}) using three aluminum electrode setup. Data were recorded during the fifth cycle, and it typically took several cycles to reach a stable shape of the CV curve (Fig. S1). Note that our CV tests were done in pouch cell configuration, with working- and counterelectrodes separated by glass fiber paper (which was saturated with electrolyte), so that these tests would represent the battery setup we used. (*C*) Galvanostatic charge/discharge curve using $AlCl_3$/urea = 1.3 electrolyte at 100 mA g^{-1} (cycle 20). (*D*) Schematic of battery charging (Al deposition and anion intercalation in graphite).

Downloaded by guest on February 24, 2022

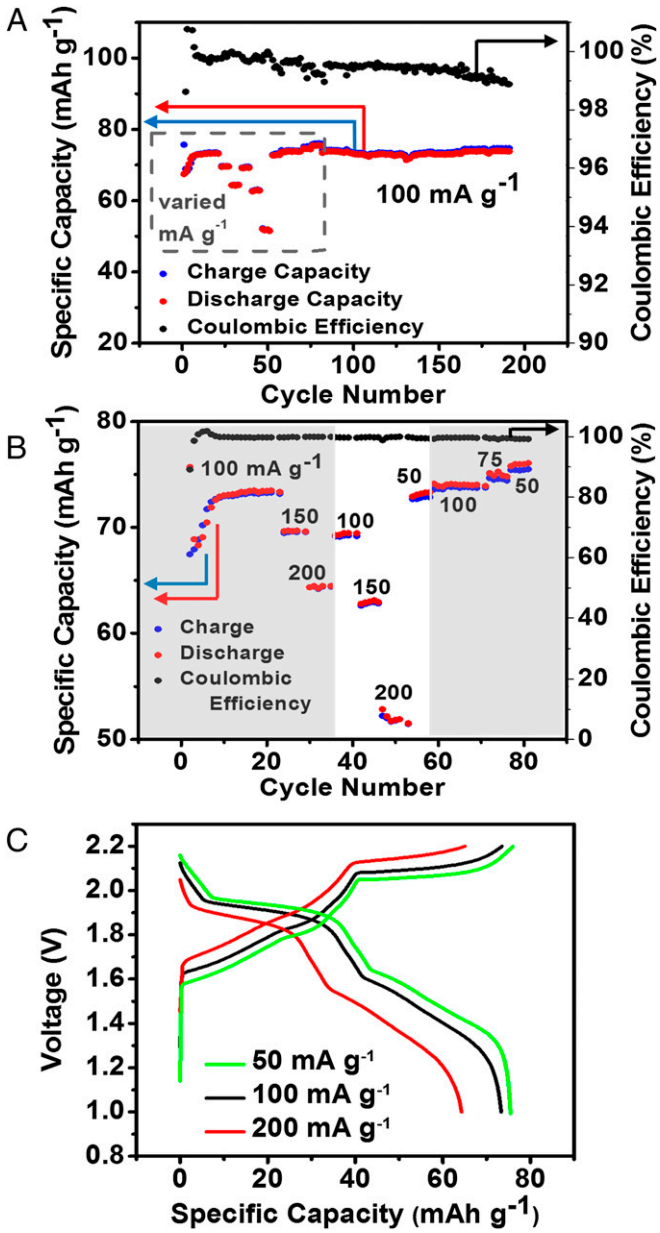

Fig. 2. Characteristics of an Al ion battery in $AlCl_3$/urea = 1.3 electrolyte. (*A*) Stability test (after charge–discharge rate variation) up to ∼180 cycles (specific current 100 mA g^{-1} and 2.2-V/1-V upper/lower cutoff). (*B*) Boxed region of *A* (cycles 1–80) with varied charge/discharge rate. Cycle regions in gray depict 2.2-V upper cutoff; region in white depicts 2.15-V upper cutoff. Lower cutoff is 1 V for all regions. (*C*) Galvanostatic charge–discharge curves for 50, 100, and 200 mA g^{-1}, 2.2-V/1-V upper/lower cutoff.

∼180 cycles. A slight decay in CE was observed over this time but it remained >99%. Despite the slight decay in Coulombic efficiency, energy efficiency increased slightly over cycling (due to increasing voltage efficiency), yielding values of 87.8% and 90.0% at specific currents of 100 mA g^{-1} or 50 mA g^{-1}, respectively. The effects of rate on the galvanostatic charge–discharge curves are shown in Fig. 2*C*, and reasonable capacities of ∼75 mAh g^{-1}, 73 mAh g^{-1}, and 64 mAh g^{-1} were obtained at 50 mA g^{-1} (0.67 C), 100 mA g^{-1} (1.4 C), and 200 mA g^{-1} (3.1 C) specific currents, respectively.

In Situ Raman Spectroscopy. In situ Raman scattering during charging/discharging experiments (*SI Materials and Methods*) were performed to investigate the changes to the graphite structure during battery operation. Fig. 3 displays spectra (Fig. 3 *A* and *C*) recorded during charge/discharge at a rate of 50 mA g^{-1} correlated to the respective regions of the galvanostatic charge/discharge curves (Fig. 3 *B* and *D*). The data were recorded in the battery's 81st charge–discharge cycle, without observing obvious increase in the graphite defect-related D band (Fig. S2), suggesting high graphite structural integrity through chloroaluminate intercalation/deintercalation cycles. Immediately upon beginning the lower plateau charging process, the G band of pristine graphite (1,584 cm^{-1}) split by ∼20 cm^{-1}. This splitting resulted from rearrangement of positive charges on the boundary layers of the graphite during intercalation. Boundary layers adjacent to intercalant layers experienced more positive charges, leading to a large blue shift in the E_{2g} band for these layers, giving rise to two different E_{2g} peaks overall, inner (i) and outer (b) (Fig. 3*A*, *Inset*; spectra in red) (16, 17). Based on the ratio of the intensities of these two peaks, the intercalation stage ($n > 2$) at that moment in time could be calculated based on the following equation:

$$\frac{I_i}{I_b} = \frac{\sigma_i}{\sigma_b}\frac{(n-2)}{2},$$

where σ_i/σ_b is the ratio of Raman scattering cross-sections, which was assumed to be unity (16). This initial splitting therefore indicated the formation of a dilute stage 4–5 intercalation compound, and as charging continued the two peaks steadily blue-shifted with increasing potential/capacity of the battery. The $E_{2g(b)}$ band then underwent a small splitting (∼3 cm^{-1}) at 1.94–1.99 V (Fig. 3*A*, *Inset,* spectra in green). At this point, the stage number (n) was calculated to be ∼2.5. Shortly afterward (at 2.03 V) the $E_{2g(i)}$ band disappeared completely. This was followed by the $E_{2g(b)}$ roughly doubling in intensity before it underwent another large splitting (1,619–1,632 cm^{-1}) at the beginning of the upper plateau (∼2.097 V) (Fig. 3*A*, spectra in blue). At the fully charged state, only one high-intensity peak at 1,632 cm^{-1} remained, suggesting the formation of a stage 1 or 2 graphite intercalation compound (GIC) because neither $E_{2g(i)}$ and $E_{2g(b)}$ bands were present (16). A stage 2 GIC was assumed, based on the capacity of the Al battery.

The subsequent discharge process was reflective of the charge process, demonstrating reversibility. As the discharge of the upper plateau began (2.011 V), there was a slight red shift by 1 cm^{-1}. This band then split (∼12 cm^{-1}) halfway through the upper plateau (1.97 V), with another peak reappearing at 1,619 cm^{-1}. The 1,631-cm^{-1} peak proceeded to completely disappear, and the 1,619-cm^{-1} peak maximized at ∼1.66 V, which signified the end of the upper plateau discharging process/deformation of the stage 2 GIC (Fig. 3*C*, spectra in blue). Halfway through the lower voltage plateau (1.535 V) the second large splitting occurred and the original $E_{2g(i)}$ began to reappear with decreasing potential (Fig. 3*C*, *Inset*; spectra in red). Shortly after the reappearance of the $E_{2g(i)}$ mode, another splitting occurred at 1.525–1.535 V, small in magnitude (∼5 cm^{-1}), as was seen during the charging process (Fig. 3*C*, *Inset,* spectra in green). This splitting likely corresponded to one of the several lower current redox events in this region demonstrated by CV (Fig. 1*A*). Of course, all bands red-shifted during discharge.

Speciation in Electrolyte by Raman Spectroscopy. Next, we investigated the speciation in several $AlCl_3$/urea electrolytes. In the $AlCl_3$/urea = 1.0 ILA electrolyte, it was suggested (3) that aluminum deposition must have occurred from a cationic species of the form $[AlCl_2{\cdot}(ligand)_n]^+$, because $Al_2Cl_7^-$ was not present and $AlCl_4^-$ cannot be reduced in the relevant voltage window. We performed Raman spectroscopy studies of five electrolytes with $AlCl_3$/urea in the range of 1.0–1.5 (Fig. 4*A*). Raman spectroscopy has previously been used to reveal the existence of chloroaluminate anions in both ILs (18–20) and ILAs (21, 22), with the Raman shifts appearing rather invariant in both ILs or ILAs with different cationic species. We observed characteristic

Downloaded by guest on February 24, 2022

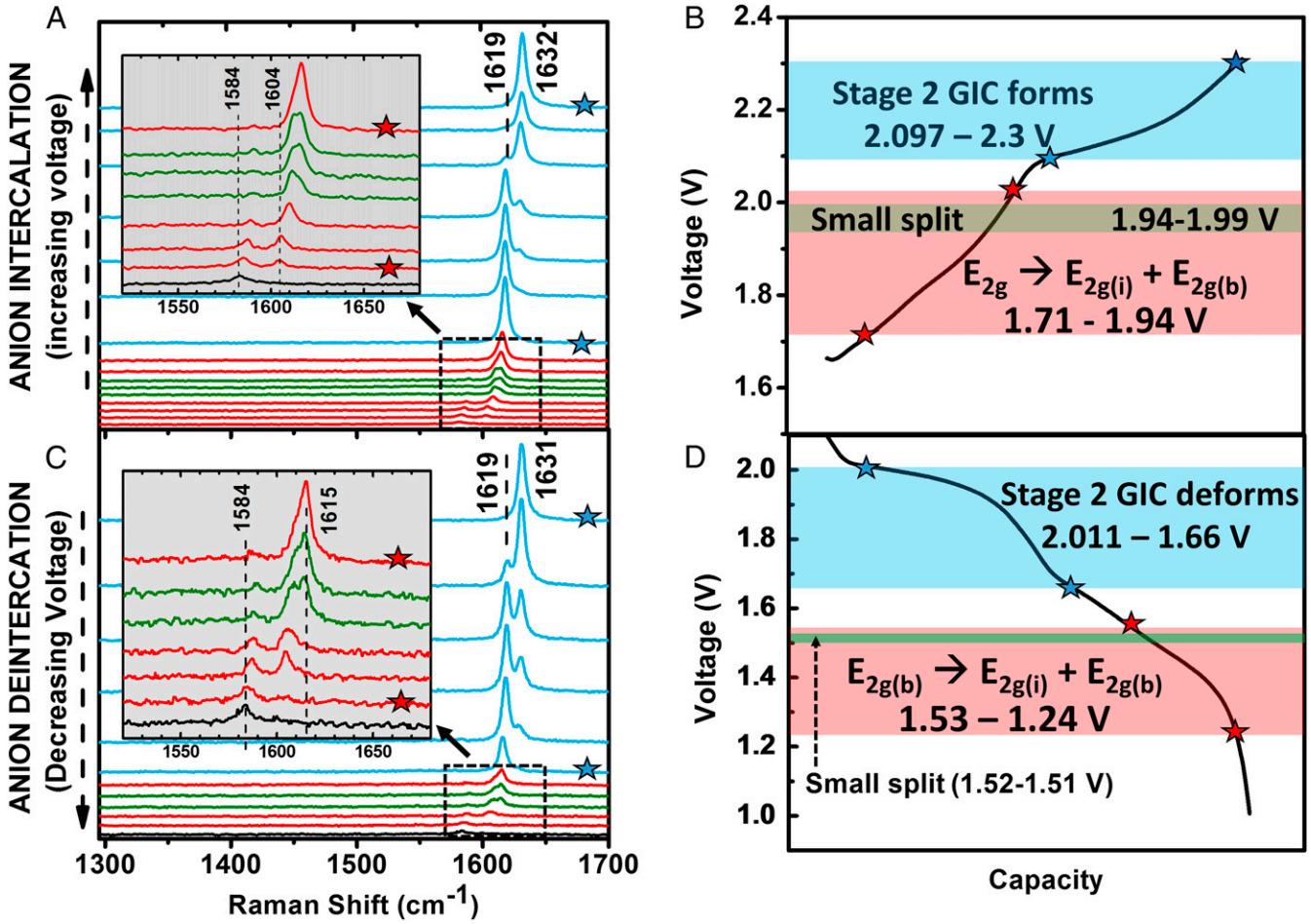

Fig. 3. In situ Raman spectra of the graphite electrode recorded during (*A*) charge and (*C*) discharge at 50 mA g^{-1}. (*Insets*) Zoom-ins on lower voltage spectra corresponding to graphite G band $E_{2g} \rightarrow E_{2g(i)} + E_{2g(b)}$ splitting (spectra in red, corresponding to red-shaded section of charge/discharge curves; spectra in green, corresponding to green-shaded section of charge/discharge curves). The black spectrum in each corresponds to open circuit voltage = 1 V, G band = 1,584 cm^{-1}. Spectra in blue (corresponding to upper plateau, shaded in blue on charge/discharge curves) represent stage 2 GIC formation/deformation. (*B*) Galvanostatic charging curve (50 mA g^{-1}), color coordinated with Raman spectra in *A*. (*D*) Galvanostatic discharging curve (50 mA g^{-1}) color coordinated with Raman spectra in *C*.

Raman shifts of $AlCl_4^-$ (311 cm^{-1}) and $Al_2Cl_7^-$ (347 cm^{-1}) for $AlCl_3$/urea >1.0. For the $AlCl_3$/urea = 1.0 electrolyte, only the 347-cm^{-1} peak ($AlCl_4^-$) was present, supporting the absence of $Al_2Cl_7^-$. When more $AlCl_3$ was added (increasing to 1.1, 1.3, 1.4, 1.5 ratios), the peak at 310 cm^{-1} ($Al_2Cl_7^-$) systematically intensified relative to 347 cm^{-1}, suggesting the existence of $Al_2Cl_7^-$. Additionally, we observed less-intense modes of $Al_2Cl_7^-$ that also increased with $AlCl_3$ content (Fig. 4*B*) (19).

Because $Al_2Cl_7^-$ exists in our $AlCl_3$/urea = 1.3 electrolyte used for the Al battery, aluminum deposition likely occurs through two pathways (3, 9):

$$\text{Negative electrode reaction}: 4\,Al_2Cl_7^- + 3\,e^- \rightarrow Al + 7\,AlCl_4^-, \quad [1]$$

$$\text{Negative electrode reaction}: 2\,[AlCl_2 \cdot (urea)_2]^+ + 3\,e^- \rightarrow Al + AlCl_4^- + 4\,(\text{urea}), \quad [2]$$

where deposition through a cationic species would likely be dominant (Eq. **2**). During aluminum deposition, cationic species would migrate to the aluminum electrode, whereas anionic species would migrate to the graphite electrode. Furthermore, Al deposition from the cation (via Eq. **2**) generates free urea at the surface of the aluminum electrode, which would likely react with some amount of $Al_2Cl_7^-$. Eq. **2** assumes that only a four-coordinate cation exists, in which two urea molecules are bound to Al by the oxygen atom in urea (3). The tricoordinate cation is unlikely due to the lack of inductive substituents on the nitrogen of urea that might allow it to be bidentate, as is seen in the case of acetamide derivatives (21). The graphite intercalation reaction remains the same as in the EMIC-$AlCl_3$ Al battery case regardless of the aluminum stripping process at the anode:

$$\text{Positive electrode reaction}: AlCl_4^- + C_x - e^- \rightarrow C_x^+\,[AlCl_4]^-, \quad [3]$$

where x is the number of carbon atoms per intercalated anion (x = 30 based on a capacity of 75 mAh g^{-1} from 50-mA g^{-1} galvanostatic discharging data). The specific energies calculated using Eqs. **1** and **2** were 45 Wh kg^{-1} and 76 Wh kg^{-1}, respectively. These values represent an upper limit to the specific energy, as the calculation neglects the fraction of neutral species that would necessarily accompany the anionic and cationic species in this liquid, which is not 100% ionic.

Analyzing Relative Concentrations of Ionic Species in Electrolyte. We analyzed the relative concentrations of ions in the electrolyte,

Downloaded by guest on February 24, 2022

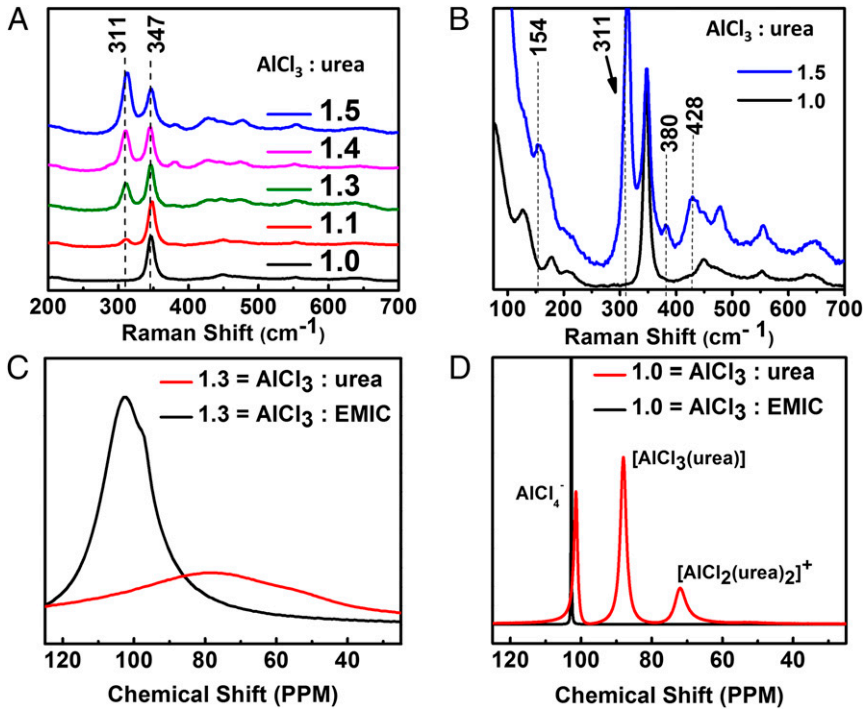

Fig. 4. Electrolyte speciation study. (*A*) Raman spectra of $AlCl_3$/urea = 1.0, 1.1, 1.3, 1.4, 1.5 electrolytes, normalized to peak at 347 cm^{-1} ($AlCl_4^-$). (*B*) Zoom of *A* to elucidate lower intensity modes of $Al_2Cl_7^-$ (154, 310, 380, 428 cm^{-1}), 1.3, 1.4 = $AlCl_3$/urea electrolyte spectra omitted for clarity. ^{27}Al NMR spectra for (*C*) $AlCl_3$/urea = 1.3 vs. $AlCl_3$/EMIC = 1.3 and (*D*) $AlCl_3$/urea = 1.0 vs. $AlCl_3$/EMIC = 1.0. Peak assignments based on the work of Coleman et al. (22).

namely $[Al_2Cl_7^-]/[AlCl_4^-]$ and $[AlCl_2{\cdot}(urea)_2]^+/[Al_2Cl_7^-]$ using the ratio of the intensities of the Raman peaks of $Al_2Cl_7^-$ and $AlCl_4^-$ in the electrolyte (Fig. 4*A*). The ratio of the Raman scattering cross-sections of $Al_2Cl_7^-$ and $AlCl_4^-$ anions has been derived for the 1-butyl-3-methylimidazolium chloride (BMIC)/$AlCl_3$ system (20), and we used this value to estimate $[Al_2Cl_7^-]/[AlCl_4^-] = 0.6$ and $[AlCl_2{\cdot}(urea)_2]^+/[Al_2Cl_7^-] = 2.6$ (based on charge neutrality) in the $AlCl_3$/urea = 1.3 electrolyte. This further suggests that for $AlCl_3$/urea = 1.3 the aluminum deposition would be dominated by the cationic species, which is present at 2.6 times the concentration of $[Al_2Cl_7^-]$. The upper limit of the specific energy of the real system based on only electrochemically active materials would therefore be closer to 76 Wh kg^{-1}.

We performed ^{27}Al NMR spectroscopy and found Al species (23, 24) consistent with chloroaluminate anions and a urea-coordinated cation in the electrolytes (Fig. 4 *C* and *D*). Fig. 4 *C* and *D* compare ^{27}Al NMR spectra of the $AlCl_3$-urea ILA to the $AlCl_3$-EMIC IL at the corresponding molar ratios. The spectrum of the $AlCl_3$/EMIC = 1.0 electrolyte showed a single peak corresponding to $AlCl_4^-$ (δ = 101.8 ppm) anion (Fig. 4*D*). However, the spectrum of $AlCl_3$/urea = 1.0 electrolyte showed four resonances: 52.7 ppm ($[AlCl_3{\cdot}(urea)_2]$), 71.8 ppm ($[AlCl_2{\cdot}(urea)_2]^+$), 88.0 ppm ($[AlCl_3{\cdot}(urea)]$), and 101.5 ppm ($AlCl_4^-$)—assignments based on the work of Coleman et al. (22). The resonance at 52.7 ppm was broad and low intensity and is shown clearly in Fig. S3. In the $AlCl_3$/EMIC = 1.3 electrolyte, the system is totally ionic with $AlCl_4^-$ (δ = 101.8 ppm) and $Al_2Cl_7^-$ (δ = 96.7 ppm) being the dominant species at the 1.3 ratio. In the $AlCl_3$/urea = 1.3 electrolyte, the spectrum exhibited a much broader [likely due to chemical exchange (22)] feature than the $AlCl_3$/EMIC = 1.3, spanning the region corresponding to the anionic $AlCl_4^-$, $Al_2Cl_7^-$, and cationic species $[AlCl_2{\cdot}(urea)_2]^+$, consistent with the existence of these ions in the electrolyte (Fig. 4*C*). Deconvolution of this broad resonance was performed to attempt to quantify the different species, but due to incurred difficulties the results were not considered for discussion.

Conclusion

A high-efficiency battery that is stable over ∼180 cycles and a variety of charge–discharge rates using an Al anode, graphite powder cathode, and cheap $AlCl_3$/urea ionic liquid analog electrolyte was successfully established. Intercalation/deintercalation of graphite during charging/discharging was confirmed by in situ Raman experiments, and a stage 2 GIC was observed. Reversibility of the process was confirmed by recovery of the G band at 1,584 cm^{-1} with no increase of the D-band intensity observed. Raman spectroscopy and ^{27}Al NMR of the electrolyte suggested the presence of $AlCl_4^-$, $[AlCl_2{\cdot}(urea)_n]^+$ and $Al_2Cl_7^-$ ionic species in the electrolyte.

The future prospects of the Al battery based on the $AlCl_3$/urea electrolyte are promising and deserve further investigation. The high Coulombic efficiency of the battery suggests long cycling capabilities, but this (ideally thousands of cycles) must be demonstrated. The earth abundance and low-cost nature of the components of this battery make it a very attractive option for use on large scales, and its relatively low specific energy (with respect to LIBs) is acceptable for nonmobile energy storage units. The rate capability of this battery is markedly less impressive than that of the EMIC-based battery system due to the higher viscosity and lower conductivity/ionicity of the electrolyte, but should have room for further improvement. Whereas this work represents a satisfying step forward, exploration of numerous combinations of electrolytes and electrode materials remains wide open for further development of Al batteries to achieve ultrahigh specific energy/cost ratios.

Materials and Methods

SI Materials and Methods explains in detail the materials used and methods followed in this paper.

ACKNOWLEDGMENTS. H.D. acknowledges support from the US Department of Energy DOE DE-SC0016165. B.-J.H. acknowledges support from the Global Networking Talent 3.0 Plan (NTUST 104DI005) from the Ministry of Education of Taiwan. M.-C.L. acknowledges support from the Taishan Scholar Project for Young Scholars of Shandong Province of China.

Downloaded by guest on February 24, 2022

1. Yang Z, et al. (2011) Electrochemical energy storage for green grid. *Chem Rev* 111(5):3577–3613.
2. Hogg JM, Coleman F, Ferrer-Ugalde A, Atkins MP, Swadzba-Kwasny M (2015) Liquid coordination complexes: A new class of Lewis acids as safer alternatives to BF_3 in synthesis of polyalphaolefins. *Green Chem* 17(3):1831–1841.
3. Abood HMA, Abbott AP, Ballantyne AD, Ryder KS (2011) Do all ionic liquids need organic cations? Characterisation of $[AlCl2{\cdot}n\text{Amide}]^+$ $AlCl_4^{(-)}$ and comparison with imidazolium based systems. *Chem Commun (Camb)* 47(12):3523–3525.
4. Fang Y, et al. (2015) An $AlCl_3$ based ionic liquid with a neutral substituted pyridine ligand for electrochemical deposition of aluminum. *Electrochim Acta* 160:82–88.
5. Fang Y, Jiang X, Sun XG, Dai S (2015) New ionic liquids based on the complexation of dipropyl sulfide and $AlCl_3$ for electrodeposition of aluminum. *Chem Commun (Camb)* 51(68):13286–13289.
6. Pulletikurthi G, Boedecker B, Borodin A, Weidenfeller B, Endres F (2015) Electrodeposition of al from a 1-butylpyrrolidine-$AlCl_3$ ionic liquid. *Prog Nat Sci* 25(6):603–611.
7. Lin MC, et al. (2015) An ultrafast rechargeable aluminium-ion battery. *Nature* 520(7547):325–328.
8. Wu Y, et al. (2016) 3D graphitic foams derived from chloroaluminate anion intercalation for ultrafast aluminum-ion battery. *Adv Mater* 28(41):9218–9222.
9. Wilkes JS, Levisky JA, Wilson RA, Hussey CL (1982) Dialkylimidazolium chloroaluminate melts - a new class of room-temperature ionic liquids for electrochemistry, spectroscopy, and synthesis. *Inorg Chem* 21(3):1263–1264.
10. Jung SC, Kang Y, Yoo D, Choi JW, Han Y (2016) Flexible few-layered graphene for the ultrafast rechargeable aluminum-ion battery. *J Phys Chem C* 120(25):13384–13389.
11. Jayaprakash N, Das SK, Archer LA (2011) The rechargeable aluminum-ion battery. *Chem Commun (Camb)* 47(47):12610–12612.
12. Sun XG, et al. (2016) Polymer gel electrolytes for application in aluminum deposition and rechargeable aluminum ion batteries. *Chem Commun (Camb)* 52(2):292–295.
13. Wang W, et al. (2013) A new cathode material for super-valent battery based on aluminium ion intercalation and deintercalation. *Sci Rep* 3:3383.
14. Li J, Ma C, Chi M, Liang C, Dudney NJ (2015) Solid electrolyte: The key for high-voltage lithium batteries. *Adv Energy Mater* 5(4):1401408.
15. Smith AJ, Burns JC, Trussler S, Dahn JR (2010) Precision measurements of the coulombic efficiency of lithium-ion batteries and of electrode materials for lithium-ion batteries. *J Electrochem Soc* 157(2):A196–A202.
16. Balabajew M, et al. (2016) In-situ Raman study of the intercalation of bis(trifluoromethylsulfonyl) imid ions into graphite inside a dual-ion cell. *Electrochim Acta* 211:679–688.
17. Nemanich R, Solin S, Guerard D (1977) Raman-scattering from intercalated donor compounds of graphite. *Phys Rev B* 16(6):2665–2672.
18. Gale R, Gilbert B, Osteryoung R (1978) Raman-spectra of molten aluminum-chloride - 1-butylpyridinium chloride systems at ambient-temperatures. *Inorg Chem* 17(10): 2728–2729.
19. Takashi S, Curtiss L, Gosztola D, Koura N, Saboungi M (1995) Molecular-orbital calculations and Raman measurements for 1-ethyl-3-methylimidazolium chloroaluminates. *Inorg Chem* 34(11):2990–2993.
20. Gilbert B, Olivier-Bourbigou H, Favre F (2007) Chloroaluminate ionic liquids: From their structural properties to their applications in process intensification. *Oil Gas Sci Technol* 62(6):745–759.
21. Hu P, et al. (2016) Structural and spectroscopic characterizations of amide-$AlCl_3$-based ionic liquid analogues. *Inorg Chem* 55(5):2374–2380.
22. Coleman F, Srinivasan G, Swadźba-Kwaśny M (2013) Liquid coordination complexes formed by the heterolytic cleavage of metal halides. *Angew Chem Int Ed Engl* 52(48): 12582–12586.
23. Derouault J, Granger P, Forel M (1977) Spectroscopic investigation of aluminum trihalide-tetrahydrofuran complexes. 2. Solutions of aluminum-chloride or bromide in tetrahydrofuran and in tetrahydrofuran-dichloromethane. *Inorg Chem* 16(12): 3214–3218.
24. Gray J, Maciel G (1981) Al-27 nuclear magnetic-resonance study of the room-temperature melt $AlCl_3$-normal-butylpyridinium chloride. *J Am Chem Soc* 103(24): 7147–7151.

Downloaded by guest on February 24, 2022